Influence of lateral boundaries on transport in quasi-two-dimensional flow

Lei Fang and Nicholas T. Ouellette[a)]
Department of Civil and Environmental Engineering, Stanford University, Stanford, California 94305, USA

We assess the impact of lateral coastline-like boundaries on mixing and transport in a laboratory quasi-two-dimensional turbulent flow using a transfer-operator approach. We examine the most coherent sets in the flow, as defined by the singular vectors of the transfer operator, as a way to characterize its mixing properties. We study three model coastline shapes: a uniform boundary, a sharp embayment, and a sharp headland. Of these three, we show that the headland affects the mixing deep into the flow domain because it has a tendency to pin transport barriers to its tip. Our results may have implications for the siting of coastal facilities that discharge into the ocean.

Geophysical flows, such as those in the ocean, can be well approximated as two-dimensional on large scales. Two-dimensional flows in turn are particularly prone to producing a range of coherent structures that are thought to be important for determining mixing, transport, and dynamics. How such structures interact with lateral boundaries such as coastlines, however, is not well understood. In particular, it is not known how far into the flow the impact of a particular coastal feature may be felt. Here, we use a laboratory quasi-two-dimensional flow to study this question. We evaluate the impact of three different model coastlines—a uniform boundary, a sharp embayment, and a sharp headland—on coherent structures and mixing in the flow. The coherent structures are found using a transfer-operator approach, which we adapt for use in an experimental context. Our results may have implications for the siting of coastal facilities that discharge into the ocean and that must ensure appropriate mixing.

I. INTRODUCTION

At large scales, many geophysical flows, such as geostrophic flows in the oceans and atmosphere, are approximately two-dimensional (2D). This reduced dimensionality is well known to lead to a wide range of dynamical consequences, from the introduction of an infinite number of new (inviscidly) conserved quantities[1] to an inverted turbulent energy cascade[2–4] to an enhanced tendency to generate so-called *coherent structures*[5,6]. Because of both this connection to geophysical flows and their intrinsic fundamental interest, there has thus been a significant amount of work done over the past few decades on two-dimensional flows[1].

In particular, two-dimensional flows have become paradigmatic systems for the study of coherent structures, particularly from Lagrangian standpoint. A wide range of methods have been developed to find such structures, including geometric methods based on various properties of the Cauchy–Green strain tensors[7–9], probabilistic and set-oriented methods based on transfer operators[10–13], and topological methods based on the braiding of trajectories[14,15]. Although such structures likely play some role in the dynamics of the flow[6,16,17], they have been much more widely studied in the context of transport and mixing.

Most of the work on coherent structures in two-dimensional flows has focused on unbounded flows with no lateral boundaries. Real geophysical flows, however, are almost always bounded; the ocean, for example, is surrounded by coastlines. A full understanding of the effect of coherent structures on transport therefore requires the exploration of the interaction between these structures and boundaries. Some previous work in both laboratory[18] and observational[19] studies has suggested that coherent structures can sometimes be pinned to boundary features, suggesting that the influence of the boundary on transport may be felt far into the bulk of the flow. Knowledge of how fixed boundaries affect mixing could have important ramifications, for example, for the siting of coastal facilities that discharge waste products into the ocean[20,21]. Much work remains to be done, however, to characterize the effects of boundaries on transport in two-dimensional flows fully so that accurate predictions can be made in applied situations.

Here, we make progress toward this goal via controlled laboratory experiments in a quasi-two-dimensional, weakly turbulent flow in the presence of three canonical lateral boundary shapes: a uniform boundary, a model embayment, and a model headland. These boundaries are placed far from the walls of our experimental apparatus so that we can isolate their influence. We characterize the effects of the boundaries on the mixing properties of the flow using a transfer operator approach. We find that the presence of the boundaries can affect the mixing relatively far into the flow, and that headlands have a longer-range effect than embayments. In addition, we also suggest several additions to the standard transfer operator implementation to make the approach both more suitable for experimental situations, where temporal and spatial scales and resolution are fixed, and to make its

a)Electronic mail: nto@stanford.edu

This manuscript was accepted by Chaos. Click here to see the version of record.

results more interpretable.

We begin below by presenting a description of our experiment and our methods for computing and analyzing transfer operators in Section II. In Section III, we discuss our results, including both our additions to the standard transfer-operator framework and the effects of boundaries on the mixing in the flow. Finally, in Section IV, we summarize and put our results into context.

II. METHODOLOGY

A. Experimental details

To create a quasi-two-dimensional flow in the laboratory, we use an electromagnetically driven thin-layer apparatus. As we have described elsewhere in detail[22–24], our apparatus contains a thin layer (about 0.5 cm deep) of electrolytic fluid supported by a flat glass substrate. The lateral dimensions of the working fluid were 86×86 cm^2. The electrolyte itself was a solution of 14% by weight NaCl in deionized water, with density $\rho = 1.101$ g/cm^3 and viscosity 1.25×10^{-2} cm^2/s. The glass floor was coated with a hydrophobic wax to reduce friction. We also floated an additional layer, 10 mm deep, of fresh water above the electrolyte; the miscible density interface between the two fluids defines the horizontal plane we study.

Under the glass floor lies an array of 34×34 permanent magnets with diameters of 12.7 mm, thicknesses of 3.2 mm, and a center-to-center spacing of $L_m = 25.4$ mm. The strength of each magnet is roughly 600 gauss, and the magnets are arranged in stripes of alternating polarity. A DC electric current of 3.30 A is passed laterally through the thin layer of the electrolyte via a pair of copper electrodes. The coupling of the magnetic field and electric current produces a Lorentz body force on the fluid, which drives a flow that is nearly entirely in the plane. We keep the body force large enough to produce complex spatiotemporal dynamics and weak turbulence but not so large as to produce significant out of plane motions[22]. We define a bulk Reynolds number as $\mathrm{Re} = u' L_m/\nu$, where u' is the in-plane root-mean-square velocity and ν is the kinematic viscosity of the electrolyte. In the experiments described below, the Reynolds number is 200.

We measured the flow using particle-tracking velocimetry (PTV)[22,25]. The fluid was seeded with fluorescent polystyrene tracer particles with diameters of 110 μm that are small enough to follow the flow accurately, with a Stokes number of $\mathcal{O}(10^{-4})$[26]. The mass density of the tracer particles lay between those of the fresh water and the electrolyte, so that they remained at the interface between the two. We illuminated the tracer particles with LED lamps and imaged their motion with a PointGrey Flea 3 digital camera placed 50 cm above the apparatus at a rate of 60 frames per second. The 1280×1024 pixels of the camera sensor recorded a field of view of 24.5×19.36 cm^2 (about $9.5L_m \times 7.5L_m$) in the center of the apparatus, far from its walls. Each camera image contained about 22,000 particles, so that the velocity was well resolved in space. To reconstruct velocity fields, we projected the velocities measured at the particle locations onto a basis of streamfunction eigenmodes[22]. In addition to ensuring that the velocity is incompressible in the plane, this procedure also removes noise from the measured fields in way that maintains the spectral properties of the field.

As described in the introduction, our goal here is to study the interplay between transport and mixing in the flow and lateral boundaries. To that end, we constructed three canonical removable boundaries, as shown in fig. 1, which we will refer to for convenience as "coastlines": a control case of a uniform, featureless boundary, a sharp triangular embayment, and a sharp triangular headland. Both the embayment and the headland were right triangles with a peak-to-base distance of L_m. In the results reported here, the model coastlines were placed in the measurement region in the center of the apparatus (as described above) and oriented such that the alongshore direction was perpendicular to the magnet stripes. We also ran experiments for other coastline orientations, with qualitatively similar results. Finally, we note that in reconstructing the velocity field, we enforce no-flux and no-slip conditions on the coastlines[22,27].

B. Transfer-operator-based partitioning

There are of course many different ways to assess fluid mixing. Here, our specific goal is to understand the spatial structure of mixing and its relationship with coherent structures, and how these are affected by the presence of different kinds of lateral boundary conditions. Thus, it makes sense to use a mixing assessment that takes into account this structure, ideally from a Lagrangian perspective. Many Lagrangian techniques exist to study mixing that each have their strengths and weaknesses[28]. Here, we choose to take an approach based on transfer operators[11], as it allows us, via a flow partitioning, to make a relatively simple characterization of the modifications of the mixing properties of the flow by the boundary conditions while averaging over much of the inherent complexity of the turbulent flow. Additionally, the solid mathematical foundation of the transfer operator allows us to make estimates of relevant time scales, as we describe more fully below.

Formally, the transfer operator maps a density initially located in some region of the flow X to a (possibly) different region Y. Here, we follow Froyland *et al.*[11] and use a finite-dimensional numerical approximation of the transfer operator. We first break up the initial domain X into subsets B_i and the final domain Y into subsets C_j, and then define the transfer operator as

$$\boldsymbol{P}^{(\tau)}(t)_{i,j} = \frac{\ell(B_i \cap \Phi(C_j, t+\tau; -\tau))}{\ell(B_i)}. \qquad (1)$$

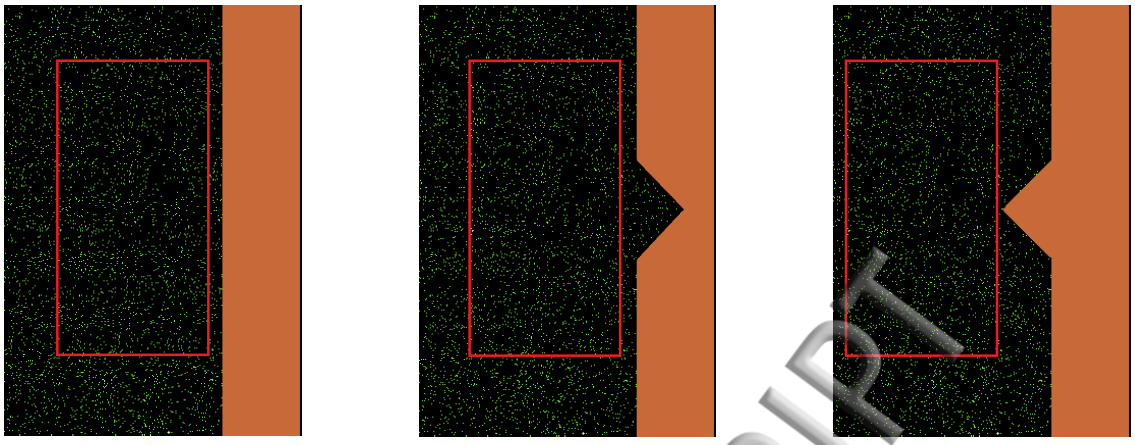

(a) (b) (c)

FIG. 1. Sketches of the three boundary shapes used in this work: (a) a uniform lateral boundary, (b) a sharp embayment, and (c) a sharp headland. In these images, the magnet stripes are horizontal. The boxes show the region in which transfer operators and flow partitions were computed.

Here, $\Phi(\mathbf{z}, t, \tau)$ is the flow map, which gives the location of a fluid element at time $t+\tau$ that was at position $\mathbf{z}$ at time t, and ℓ is a normalized volume measure. Thus, since $\boldsymbol{P}^{(\tau)}(t)_{i,j}$ is row-stochastic by construction, it encodes the probability that a fluid element initially in B_i at time t will be found in C_j after being advected by the flow for a time τ.

Again following Froyland *et al.*[11], we estimate the transfer operator in our experimental data by first breaking our flow domain into a grid of 25×25 boxes; these boxes are the B_i in eq. 1. We are interested here in coherent mixing within the domain rather than transport from one part of the flow to another; thus, we set the C_j to be the same boxes as the B_i. We place $N_p = 200$ virtual Lagrangian points $\mathbf{z}$ uniformly in each of the B_i at time t, which we advect forward to time $t+\tau$ by integrating their equations of motion through the experimentally measured velocity fields using a second-order Runge–Kutta integrator[26]. We can then approximate the transfer operator by simply counting: the value of $\boldsymbol{P}^{(\tau)}(t)_{i,j}$ is given by the ratio of the number of particles that begin in B_i at time t and end in C_j at time $t+\tau$ to N_p, the total number of particles that began in B_i[11]. Although using a grid of 25×25 boxes to approximate the transfer operator is coarser than might be ideal, we are limited by the finite spatial resolution in the experiment: if the grid is too fine, then the velocity field felt by the virtual Lagrangian points inside each box will primarily be interpolated between the measured data points, leading to errors. To test this, we tried varying the number of boxes in the grid, and found that 25×25 was a good compromise between accuracy and resolution. As another test, we also tried using a square domain rather than a rectangular domain to test for possible biases due to the domain shape. This change did not, however, qualitatively affect our results.

With this approximation of the transfer operator in hand, we can use it to partition the flow domain into its most coherent subsets, which we label X_1 and X_2 at time t and Y_1 and Y_2 at the final time $t+\tau$, such that $X = X_1 \cup X_2$ and $Y = Y_1 \cup Y_2$. Note that Y_1 is the image of X_1 and Y_2 is the image of X_2 under the flow map. Froyland *et al.*[11] constrain this partitioning by requiring the measure of each subset to be about half of the full set and that the extracted subsets be the most coherent in a sense that is defined by the properties of the transfer operator. Specifically, they first define diagonal matrices Π_p and Π_q, where the diagonal entries of Π_p are the number of Lagrangian points in each of the B_i (normalized by the total number of points in the calculation, $25 \times 25 \times 200$ in our case) and the diagonal entries of Π_q are the (normalized) number of Lagrangian points in each of the C_j. They then form the matrix $\Pi_p^{1/2} P \Pi_q^{-1/2}$, where P is the discrete estimate of the transfer operator, and compute its singular values and singular vectors. We label the singular values as σ_n, where σ_1 is the largest singular value (which is always 1, by construction), and so on. Denoting the left and right singular vectors corresponding to the second-largest singular value σ_2 as $\hat{x}$ and $\hat{y}$, respectively, one then defines

$$\begin{aligned} x &= \hat{x}\Pi_p^{-1/2}, \\ y &= \hat{y}\Pi_q^{-1/2}. \end{aligned} \tag{2}$$

Visually inspecting these vectors can give a fuzzy, qualitative sense of the most coherent sets in the flow. The more positive x_i is, the more likely it is to belong to X_1; and the more negative it is, the more likely it is to belong to X_2 (with an analogous relationship between y_i, Y_1, and Y_2). Values of x_i close to zero are more am-

This manuscript was accepted by Chaos. Click here to see the version of record.

biguous. Nevertheless, one can then use these vectors to create a binary partition of the flow domain via

$$X_1 = \bigcup_{i:x_i>b} B_i, \quad X_2 = \bigcup_{i:x_i<b} B_i \tag{3}$$

$$Y_1 = \bigcup_{j:y_j>c} C_j, \quad Y_2 = \bigcup_{j:y_j<c} C_j. \tag{4}$$

b and c here are free parameters that allow one to balance the number of points sorted into each part of the partition, and one typically seeks to set them to balance the partition. Here, we simply use $b = c = 0$.

The sets computed via this method will be the most coherent in the flow, in the sense that fluid that began in X_1 will map primarily into Y_1 under the action of the flow with as little leakage into Y_2 as possible. By construction, then, the fluid initially in X_1 does not mix with the fluid initially in X_2. Thus, if we compare with the widely used methods for detecting so-called Lagrangian Coherent Structures (LCSs)[9], which seek to find co-dimension 1 transport barriers, we can think of the sets identified by this transfer-operator method as the regions of fluid that are approximately bounded by LCSs.

C. Handling open domains

So far, we have described exactly the method introduced by Froyland *et al.*[11] for partitioning the flow domain into finite-time coherent sets. However, as a practical matter, we found that we needed to introduce some modifications to make the method feasible for use in an experimental setting. As defined in eq. 1, the transfer operator depends on the time scale τ, and the partitioning of the flow will produce the sets that are the most coherent *over this time scale*. τ is thus a free parameter, and ought to be set by the flow physics. To be able to construct the transfer operator accurately, one thus needs to be able to follow the trajectories of all of the Lagrangian points introduced at time t for the entire duration τ. Most experiments and field observations, however, measure the flow field only for a subdomain of the entire body of fluid—and thus, since this measurement domain is open, the Lagrangian points may freely leave the field of view. Once an appreciable fraction of the points have left the field of view, the transfer operator can no longer be reliably constructed, both because the smaller number of particles may lead to statistical sampling issues (or even empty entries in the P matrix) and because some of the "lost" particles may actually return to the domain at some later time. Thus, the time scale τ in an experiment is limited by the field of view, and cannot necessarily be set optimally for the relevant physics.

We overcome this (experimental) limitation by calculating transfer operators only for short time intervals $\delta\tau$ for which most of the the Lagrangian points remain in the field of view. We then exploit the fact that transfer operators can be composed via matrix multiplication[29] to construct a long-time transfer operator as

$$\begin{aligned}\boldsymbol{P}^{(\tau)}(t)_{i,j} =& \boldsymbol{P}^{(\delta\tau)}(t)_{i,j} \cdot \boldsymbol{P}^{(\delta\tau)}(t+\delta\tau)_{i,j} \\ & \cdot \boldsymbol{P}^{(\delta\tau)}(t+2\delta\tau)_{i,j} \cdot \ldots \cdot \boldsymbol{P}^{(\delta\tau)}(t+(n-1)\delta\tau)_{i,j}\end{aligned} \tag{5}$$

where $\cdot$ denotes matrix multiplication and τ is the time interval lasting from t to $t + n\delta\tau$. Similar composition approaches have been successfully used previously to construct long-time flow maps from short-time maps[30]. This approach is not perfect, in part because we are only computing an approximation of the true transfer operator and small errors introduced in each short-time approximation may compound. It is, however, necessary given the realities of experimental data. And, as we show below, our results offer support for the efficacy of this approach. Finally, even for short times, a small fraction of Lagrangian points may still leave the domain. Thus, we normalize each row of the transfer operators so that they sum to unity before we multiply them together. Since transfer operators map densities, this normalization will not affect their structure as long as each box still contains enough Lagrangian points to be statistically significant. We note that because we construct long-time transfer operators from the composition of short-time operators, this loss of particles is a small effect, and so the required renormalization of the rows of the transfer operator is always less than 4%; if it were larger, a more careful, systematic approach may be needed[31].

D. Partition confidence and coherence time scales

Making the modifications to the standard transfer-operator-based flow partitioning described in the previous makes the method feasible to run on experimental data. But there still remains an issue that can make the results of the algorithm difficult to interpret, particularly in highly unsteady and complex turbulent flows where the "correct" partitioning is difficult to guess *a priori*: the method described above will *always* produce an answer (that is, a binary partitioning of the flow domain into two sets), even if this answer has little meaning.

As described above, the algorithm of Froyland *et al.*[11] partitions the flow domain using the second-largest singular value of the transfer operator σ_2, as this value is guaranteed by the Perron–Frobenius and Courant–Fischer theorems to produce the maximally coherent sets[11,32]; thus, the magnitude of σ_2 indicates the level of coherence of the sets. Note that the largest singular value of the transfer operator is always unity, and simply represents conservation of mass. If σ_2 is much larger than, say, the third-largest singular value σ_3, we can additionally assert that we are confident in the partitioning of the domain, and that a partitioning based on σ_3 would be significantly inferior. But if these singular values are close in magnitude, our confidence is much lower, since noise or uncertainty could potentially change the ordering of the singular values. Partially for this reason, other

partitioning methods based on operator spectra typically require a spectral gap larger than some threshold when identifying coherent structures[33,34].

Here, we follow these previous authors and require a gap between the second and third singular values to consider the partition to be meaningful. However, we extend this idea by exploiting the inherent time dependence in the flow. As we mentioned above, the transfer operator, and therefore the maximally coherent sets, depends on the time scale τ, which should be determined by the flow physics. But how exactly can we use the flow information to decide on τ? We suggest here that if we track the singular values over a range of τ and the spectral gap between the second and third singular values suddenly increases at some particular value of τ, then that time scale reflects an important time scale in the flow, because on that time scale we can be much more confident that a binary partitioning of the flow will be meaningful. Thus, in what follows, we enforce two criteria when reporting transfer-operator partitions: that (1) the second singular value be large enough (0.7, here) so that the partition is sufficiently coherent and (2) that the spectral gap between the second and third singular values be large as well, which may necessitate tuning of τ.

III. RESULTS

In most unsteady, turbulent flows, and certainly in those we consider here, at any given time there will be many coherent structures. In that sense, the binary partition of the flow field provided by the transfer-operator method described here is an oversimplification. However, our goal is to gain an understanding of the effects of lateral boundaries on the typical mixing properties of the flow—and for that purpose, such a partitioning is sufficient. In addition, since we are primarily interested in the "typical" effects of these boundaries, for much of the following analysis we average over several different statistically independent realizations of the flow.

A. Uniform boundary

We begin with the uniform boundary (fig. 1a) as a control case. In fig. 2, we show the transfer-operator singular values for for different mapping times τ. Clearly, the singular values decay at different rates, with the larger singular values decaying more slowly (indicating their more significant coherence). In fig. 3, we show the ratio of the second and third singular values σ_2 and σ_3 as a function of time, demonstrating that the spectral gap between them is not fixed but rather grows as time evolves. For the uniform boundary, the spectral gap appears to grow in a sequence of rapid increases followed by periods with slower change. To reiterate from above, these rapid increases indicate significant enhancement of the confidence we have in the flow partitioning. We attribute

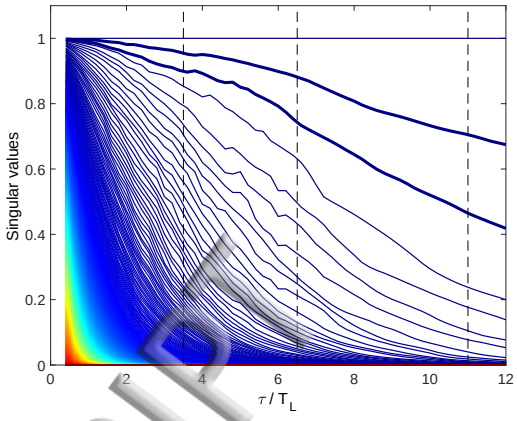

FIG. 2. Evolution of the transfer-operator singular values for the uniform boundary as a function of τ, the time span over which the transfer operator is computed, in units of the magnet-scale eddy turnover time T_L. The largest singular value is fixed at 1 by construction, but the others decay with time, indicating a loss of coherence. The second and third singular values σ_2 and σ_3 are shown by thicker lines. The vertical dashed lines show the values of τ for which flow partitions are shown in fig. 4.

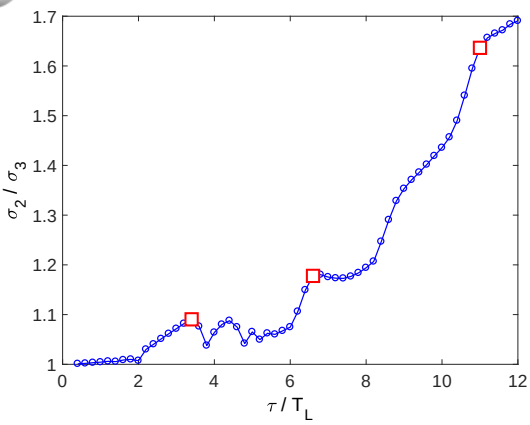

FIG. 3. The evolution of the spectral gap (that is, the ratio of the second and third singular values) as a function of the time-span τ of the transfer operator for the uniform boundary. The values of τ for which flow partitions are shown in fig. 4 are plotted with large squares.

the fluctuation in σ_2/σ_3 near $\tau = 4T_L$ to the short-time stochasticity inherent to our turbulent flow, and would expect it to be reduced by averaging over a larger ensemble. We also note that the second singular value remains above our threshold for this entire time span, indicating that the coherence of the sets it distinguishes is still large.

In fig. 4, we show the flow partitions at three values of τ, each just after one of the periods of rapid increase: $\tau \approx 3.5T_L$, $6.5T_L$, and $11T_L$, where $T_L = L_m/u'$ is the eddy turnover time of the magnet-scale eddies. In each case, we show results at both the initial time (that is,

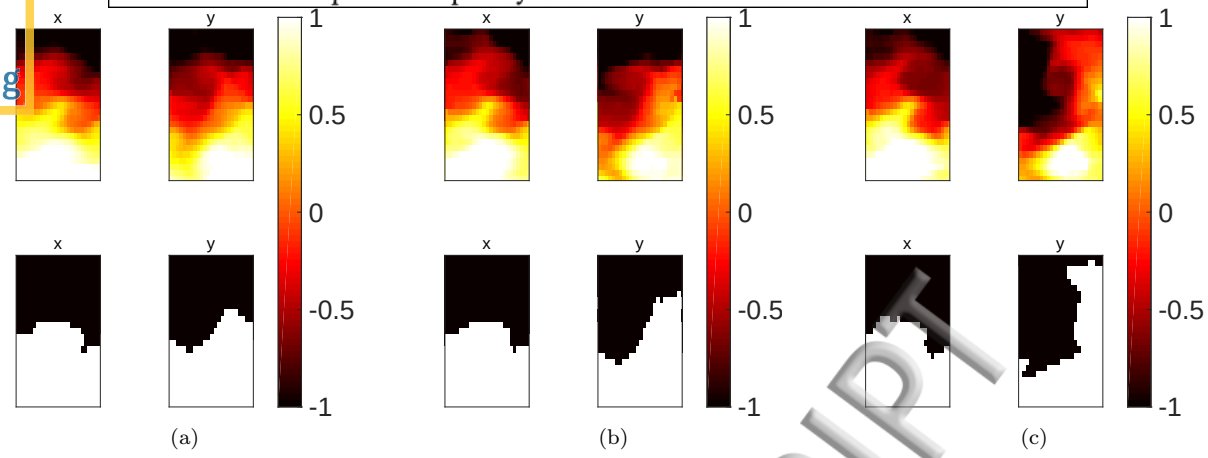

FIG. 4. Flow partition for the uniform boundary, for (a) $\tau \approx 3.5T_L$, (b) $\tau \approx 6.5T_L$, and (c) $\tau \approx 11T_L$. For each value of τ, the top two panels show the values of the singular vectors x and y, while the bottom two panels show the binary partition of the domain following Froyland *et al.*[11]. The left panels are at the initial time, while the right panels are at the final time. The boundary itself is on the right of the domain (see fig. 1(a)). The values of the second singular value σ_2 and the ratio of the second singular to the third, σ_2/σ_3, are (a) 0.94 and 1.082, (b) 0.92 and 1.149, and (c) 0.71 and 1.636.

the sets X_1 and X_2) and the final time (the sets Y_1 and Y_2) and for the "fuzzy" partitions (that is the x and y vectors defined in eq. 2) and the binary partitions following Froyland *et al.*[11]. As τ increases, we see that Y_1 and Y_2 gradually move from being separated vertically to being separated horizontally; that is, the sets flow in the along-shore direction. However, the exact position of the boundary between the two sets is somewhat fuzzy, as indicated by relatively large regions where the components of the x and y vectors are close to zero.

Physically, the uniform boundary on the right side of the domain reduces the velocity component perpendicular to it, and hence transport parallel to the boundary is enhanced. Also, we see a directional preference here. The top coherent set intrudes into the bottom one from left side, and the bottom coherent set intrudes into the top one from right side. This anisotropy is likely caused by an interaction between the background flow and the uniform boundary edges. As mentioned in Sec. II, the magnets in our apparatus are arranged in stripes, and the uniform boundary is perpendicular to the stripes. But the uniform boundary does not extend to the walls of the apparatus, but rather ends inside it (though outside the field of view of the camera). At its edges, the weak background mean flow introduced by the stripes interacts with the edges to produce a flow parallel to the boundary, which causes the directional preference here. In a previous study, we have shown that the magnet effect does appear in, for example, the long time averaged finite time Lyapunov exponent (FTLE) fields[35]. In that case, however, we had to average for a very long time to see the weak magnet effect due to the stronger turbulent fluctuations. Here, we averaged over a much smaller data set, and yet the directional preference is clearly observable. This result may indicate that the transfer operator is more sensitive to weak directional preference than FTLEs are.

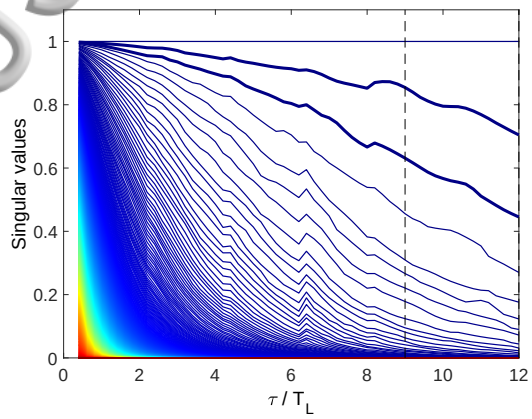

FIG. 5. Evolution of the transfer-operator singular values for the sharp embayment as a function of τ. As in fig. 2, the second and third singular values σ_2 and σ_3 are shown by thicker lines. The vertical dashed lines show the values of τ for which flow partitions are shown in fig. 7.

Finally, we note that we also performed a similar analysis on data far from any boundaries, where the flow is statistically isotropic. In that case, we found no identifiable time scales in the evolution of the spectral gap σ_2/σ_3. Additionally, the values of σ_2/σ_3 were systematically lower than for the uniform boundary case, indicating weak confidence in any computed flow partitioning, just as one would expect on the average for an unsteady isotropic flow.

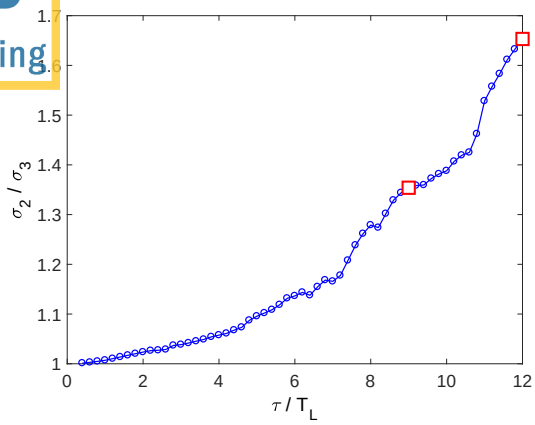

FIG. 6. The evolution of the spectral gap as a function of τ for the sharp embayment. The values of τ for which flow partitions are shown in fig. 7 are plotted with large squares.

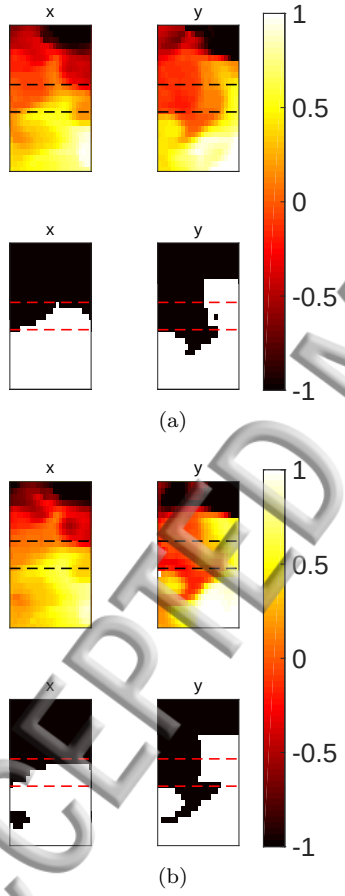

FIG. 7. Flow partition for the sharp embayment, for (a) $\tau \approx 9T_L$ and (b) $\tau \approx 12T_L$. The ordering of the panels is the same as in fig. 4, the embayment is on the right, as in fig. 1(b), and the extent of the embayment is shown by the dashed lines. The values of the second singular value σ_2 and the ratio of the second singular to the third, σ_2/σ_3, are (a) 0.74 and 1.354 and (b) 0.71 and 1.653.

B. Sharp embayment

The sharp triangular embayment (fig. 1b) behaves similarly to the uniform boundary. In fig. 5, we show the evolution of the transfer-operator singular values as a function of the advection time τ, and in fig. 6, we show the ratio of the second and third singular values. The behavior of these curves is similar to the same quantities computed for the uniform boundary case, although the growth of the spectral gap between the second and third singular values with time is somewhat smoother. Nevertheless, features in this curve are evident at $\tau \approx 9T_L$ and $12T_L$ (the end of the record), which we take to be relevant times for examining the domain partitioning. This partition is shown in fig. 7. Comparing with the uniform boundary case, a similar along-shore intrusion is apparent. However, as can be seen by looking at the x and y vectors directly rather than the binary partition, the partitioning of the domain is fuzzier in this case, and the interface between the two most coherent sets is not as sharp. This lack of sharpness is evident in the behavior of the spectral gap over time: its evolution is smoother than that of the uniform boundary with less pronounced structure, indicating a less clear separation of the two most coherent sets.

We can understand why the uniform boundary and the sharp embayment behave similarly by noting that the region inside the embayment is essentially a dead zone: there is very little flow inside it relative to the magnitude of the flow outside: we find that the root-mean-square velocity inside the embayment is only about 40% of what it is outside. However, there is still some weak coupling between the internal and external flow, which disturbs the coherent structures and is responsible for the decrease in coherence and the blurred behavior of the spectral gap in time as compared with the uniform boundary.

C. Sharp headland

Compared with the uniform boundary or the embayment, the sharp headland has a much stronger impact on the mixing in the flow. As above, we first show the evolution of the singular values for different values of τ in fig. 8 and the ratio between the second and third singular values in fig. 9. As compared with the two other boundaries we tested, the singular values decay more slowly for the headland, indicating that the coherent sets remain coherent for longer times. There is also more structure to the evolution of the spectral gap than we observed for the embayment, with much clearer features at $\tau \approx 9T_L$ and $11.5T_L$. In fig. 10, we show the flow partition at these two time scales. Although the situation is somewhat fuzzier (in that the values of the x and y vectors are closer to zero over larger regions of space), the intrusion along the boundary that we observed for both the uniform boundary and the embayment is clearly gone. Thus, we can

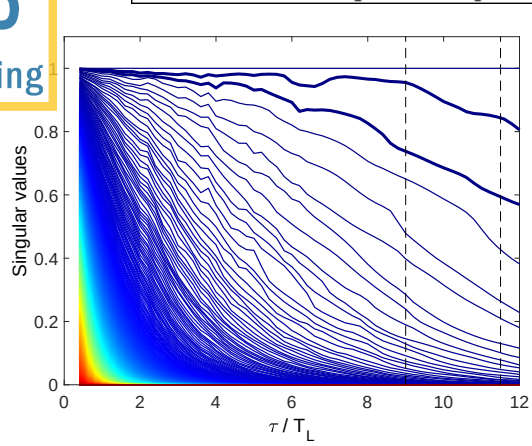

FIG. 8. Evolution of the transfer-operator singular values for the sharp headland as a function of τ. As in fig. 2, the second and third singular values σ_2 and σ_3 are shown by thicker lines. The vertical dashed lines show the values of τ for which flow partitions are shown in fig. 10.

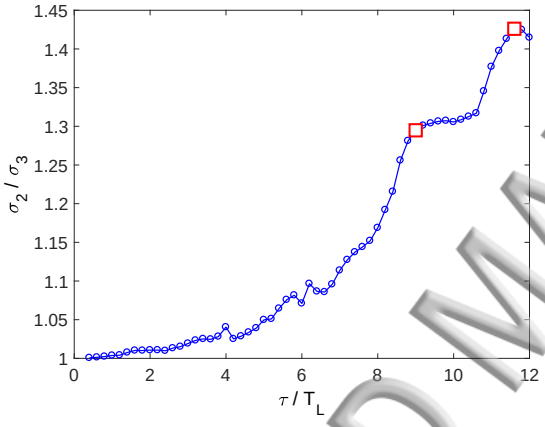

FIG. 9. The evolution of the spectral gap as a function of τ for the sharp headland. The values of τ for which flow partitions are shown in fig. 10 are plotted with large squares.

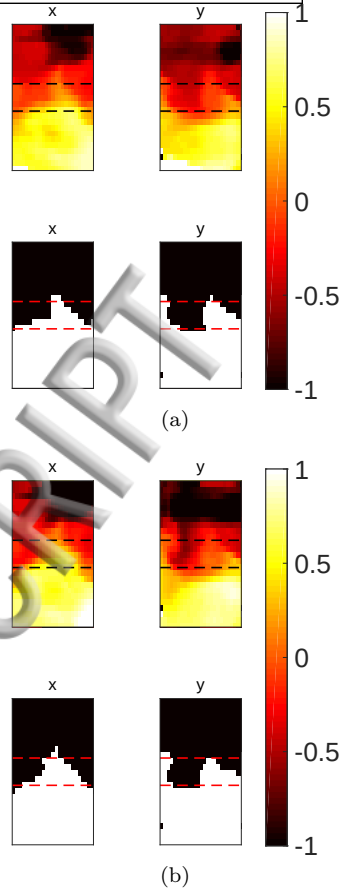

FIG. 10. Flow partition for the sharp headland, for (a) $\tau \approx 9T_L$ and (b) $\tau \approx 11.5T_L$. The ordering of the panels is the same as in fig. 4, the headland is on the right, as in fig. 1(c), and the extent of the headland is shown by the dashed lines. The values of the second singular value σ_2 and the ratio of the second singular to the third, σ_2/σ_3, are (a) 0.89 and 1.259 and (b) 0.78 and 1.426.

conclude that the headland imposes a (fuzzy) transport barrier that emanates out into the flow from its tip. We note that (as can be seen in fig. 1) the window used for computing the transfer operator and coherent sets is somewhat farther from the boundary in the headland case as compared with the uniform boundary or embayment. However, we do not expect this difference to affect our results, given that the flow in the "extra" space between the boundary and calculation window is significantly blocked by the headland and that the coherent sets we find do not show significant variation in the direction perpendicular to the boundary.

Previous theoretical and experimental work argued that separation points on boundaries can act as origination sites for Lagrangian Coherent Structures (LCSs)[18,36,37]. Our results here are consistent with this notion: the vertex of our sharp headland acts as a separation point, and LCSs are known to be transport barriers in unsteady flows[9]. The uniform boundary and embayment can also have LCSs emanating from them whenever flow separation transiently occurs; the difference here is that the vertex of the headland tends to pin LCSs to it, thus giving its attached transport barrier more statistical weight.

To ensure that our results here are an effect of the headland and not just of the orientation of the magnets, we also rotated the headland by 90°, so that its tip was oriented in the direction of the magnet stripes rather than perpendicular to them. In fig. 11, we show the flow partition for this case, computed for $\tau = 10.6T_L$. The transport barrier imposed by the headland is still present with this orientation, though (as seen from the x and y vector values) it is somewhat more fuzzy. We interpret this difference as arising from a stronger tendency of the flow to push the transport barrier in the along-shore direction in this configuration.

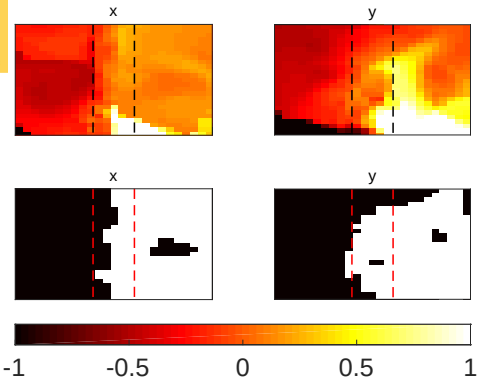

FIG. 11. Flow partition for the sharp headland orientation rotated by 90° relative to figs. 1(c) and 10, computed for $\tau \approx 10.6T_L$. In this case, the headland is on the bottom of the image, with its tip pointing up. Its extent is shown by the dashed lines. The values of the second singular value σ_2 and the ratio of the second singular to the third, σ_2/σ_3, are 0.88 and 1.087.

IV. CONCLUSIONS

We have used a transfer-operator-based approach to elucidate the effects of different lateral boundary shapes on mixing and transport in a laboratory two-dimensional flow. In addition to suggesting some modifications to the existing transfer-operator partitioning algorithm to make it more amenable to handling experimental data, we found that a uniform boundary or a model embayment had relatively small effects on the mixing, but that a sharp headland generated a statistically significant transport barrier far into the flow. This effect is likely due to a tendency of transient Lagrangian Coherent Structures to be pinned to the vertex of the headland. More generally, we also argued that evaluating the time dependence of the singular values of the transfer operator may reveal important time scales in the flow, an idea that should be extendable to situations beyond this particular study.

ACKNOWLEDGMENTS

This work was supported by the US National Science Foundation under Grant No. CMMI-1563489.

[1]G. Boffetta and R. E. Ecke, "Two-dimensional turbulence," Annu. Rev. Fluid Mech. **44**, 427–451 (2012).
[2]R. H. Kraichnan, "Inertial ranges in two-dimensional turbulence," Phys. Fluids **10**, 1417–1423 (1967).
[3]C. E. Leith, "Diffusion approximation for two-dimensional turbulence," Phys. Fluids **11**, 671–673 (1968).
[4]G. K. Batchelor, "Computation of the energy spectrum in homogeneous two-dimensional turbulence," Phys. Fluids **12**, II233–II239 (1969).
[5]P. Tabeling, "Two-dimensional turbulence: a physicist approach," Phys. Rep. **362**, 1–62 (2002).
[6]N. T. Ouellette, "On the dynamical role of coherent structures in turbulence," C. R. Physique **13**, 866–877 (2012).
[7]G. Haller and G. Yuan, "Lagrangian coherent structures and mixing in two-dimensional turbulence," Physica D **147**, 352–370 (2000).
[8]G. A. Voth, G. Haller, and J. P. Gollub, "Experimental measurements of stretching fields in fluid mixing," Phys. Rev. Lett. **88**, 254501 (2002).
[9]G. Haller, "Lagrangian Coherent Structures," Annu. Rev. Fluid Mech. **47**, 137–161 (2015).
[10]G. Froyland and K. Padberg, "Almost-invariant sets and invariant manifolds – Connecting probabalistic and geometric descriptions of coherent structures in flows," Physica D **238**, 1507–1523 (2009).
[11]G. Froyland, N. Santitissadeekorn, and A. Monahan, "Transport in time-dependent dynamical systems: Finite-time coherent sets," Chaos **20**, 043116 (2010).
[12]T. Ma and E. M. Bollt, "Relatively coherent sets as a hierarchical partition method," Intl. J. Bifurc. Chaos **23**, 1330026 (2013).
[13]G. Froyland, "An analytic framework for identifying finite-time coherent sets in time-dependent dynamical systems," Physica D **250**, 1–19 (2013).
[14]M. R. Allshouse and J.-L. Thiffeault, "Detecting coherent structures using braids," Physica D **241**, 95–105 (2012).
[15]M. Budišić and J.-L. Thiffeault, "Finite-time braiding exponents," Chaos **25**, 087407 (2015).
[16]D. H. Kelley and N. T. Ouellette, "Spatiotemporal persistence of spectral fluxes in two-dimensional weak turbulence," Phys. Fluids **23**, 115101 (2011).
[17]D. H. Kelley, M. R. Allshouse, and N. T. Ouellette, "Lagrangian coherent structures separate dynamically distinct regions in fluid flows," Phys. Rev. E **88**, 013107 (2014).
[18]M. Weldon, T. Peacock, G. B. Jacobs, M. Helu, and G. Haller, "Experimental and numerical investigation of the kinematic theory of unsteady separation," J. Fluid Mech. **611**, 1–11 (2008).
[19]M. J. Olascoaga, I. I. Rypina, M. G. Brown, F. J. Beron-Vera, H. Koçak, L. E. Brand, G. R. Halliwell, and L. K. Shay, "Persistent transport barrier on the West Florida Shelf," Geophys. Res. Lett. **33**, L22603 (2006).
[20]Y. Fernández-Torquemada, J. M. Gónzalez-Correa, A. Loya, L. M. Ferrero, M. Díaz-Vadés, and J. L. Sánchez-Lizaso, "Dispersion of brine discharge from seawater reverse osmosis desalination plants," Desal. Wat. Treat. **5**, 137–145 (2009).
[21]B. R. Hodges, J. E. Furnans, and P. S. Kulis, "Thin-layer gravity current with implications for desalination brine disposal," J. Hydraul. Eng. **137**, 356–371 (2011).
[22]D. H. Kelley and N. T. Ouellette, "Onset of three-dimensionality in electromagnetically forced thin-layer flows," Phys. Fluids **23**, 045103 (2011).
[23]Y. Liao and N. T. Ouellette, "Spatial structure of spectral transport in two-dimensional flow," J. Fluid Mech. **725**, 281–298 (2013).
[24]L. Fang and N. T. Ouellette, "Multiple stages of decay in two-dimensional turbulence," Phys. Fluids **29**, 111105 (2017).
[25]N. T. Ouellette, H. Xu, and E. Bodenschatz, "A quantitative study of three-dimensional Lagrangian particle tracking algorithms," Exp. Fluids **40**, 301–313 (2006).
[26]N. T. Ouellette, P. J. J. O'Malley, and J. P. Gollub, "Transport of finite-sized particles in chaotic flow," Phys. Rev. Lett. **101**, 174504 (2008).
[27]F. Lekien, C. Coulliette, R. Bank, and J. Marsden, "Open-boundary modal analysis: Interpolation, extrapolation, and filtering," J. Geophys. Res. **109**, C12004 (2004).
[28]A. Hadjighasem, M. Farazmand, D. Blazevski, G. Froyland, and G. Haller, "A cricital comparison of Lagrangian methods for coherent structure detection," Chaos **27**, 053104 (2017).
[29]G. Froyland and K. Padberg-Gehle, "Almost-invariant and finite-time coherent sets: Directionality, duration, and diffusion," in *Ergodic Theory, Open Dynamics, and Coherent Structures*, edited by W. Bahsoun, C. Bose, and G. Froyland (Springer New

York, New York, NY, 2014) pp. 171–216.
[30]D. M. Luchtenburg, S. L. Brunton, and C. W. Rowley, "Long-time uncertainty propagation using generalized polynomial chaos and flow map composition," J. Comput. Phys. **274**, 783–802 (2014).
[31]G. Froyland, P. K. Pollett, and R. M. Stuart, "A closing scheme for finding almost-invariant sets in open dynamical systems," J. Comput. Dyn. **1**, 135–162 (2014).
[32]R. A. Horn and C. R. Johnson, *Matrix Analysis* (Cambridge University Press, 2012).
[33]A. Hadjighasem, D. Karrasch, H. Teramoto, and G. Haller, "Spectral-clustering approach to Lagrangian vortex detection," Phys. Rev. E **93**, 063107 (2016).
[34]K. L. Schlueter-Kuck and J. O. Dabiri, "Coherent structure colouring: identification of coherent structures from sparse data using graph theory," J. Fluid Mech. **811**, 468–486 (2017).
[35]N. T. Ouellette, C. A. R. Hogg, and Y. Liao, "Correlating Lagrangian structures with forcing in two-dimensional flow," Phys. Fluids **28**, 015105 (2016).
[36]G. Haller, "Exact theory of unsteady separation for two-dimensional flows," J. Fluid Mech. **512**, 257–311 (2004).
[37]F. Lekien and G. Haller, "Unsteady flow separation on slip boundaries," Phys. Fluids **20**, 097101 (2008).

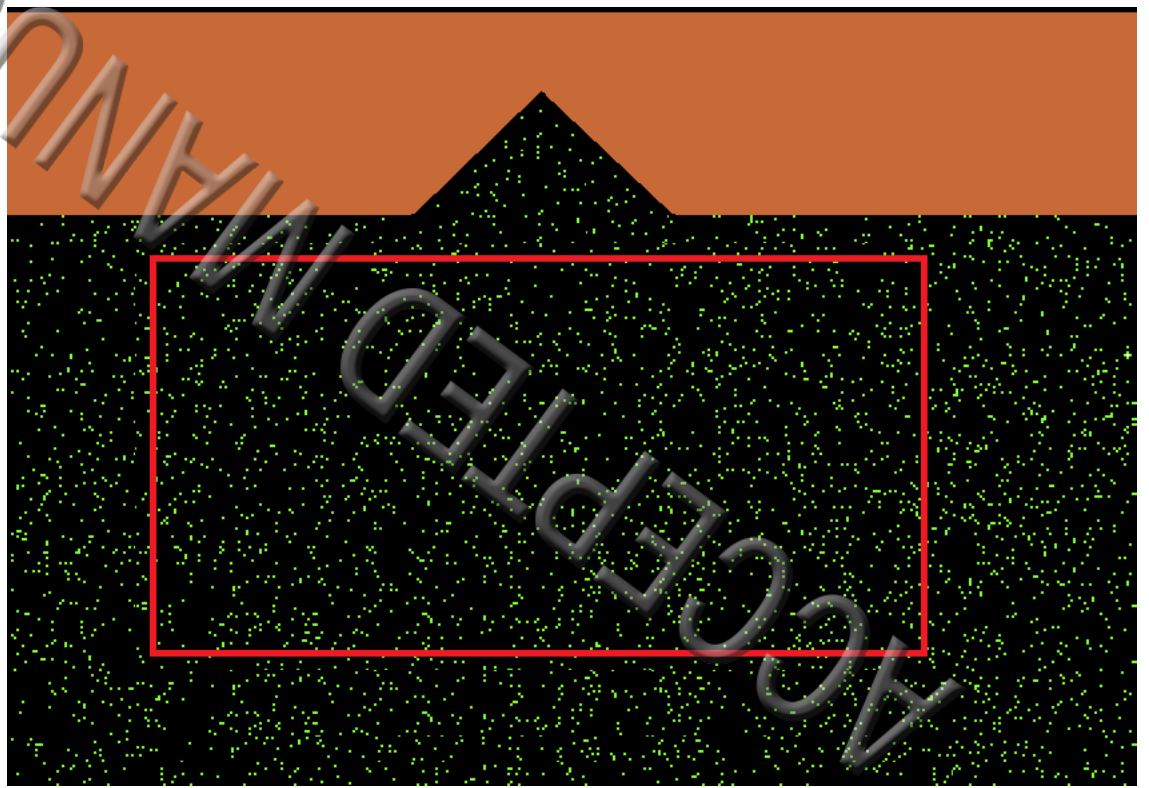
ACCEPTED MANUSCRIPT

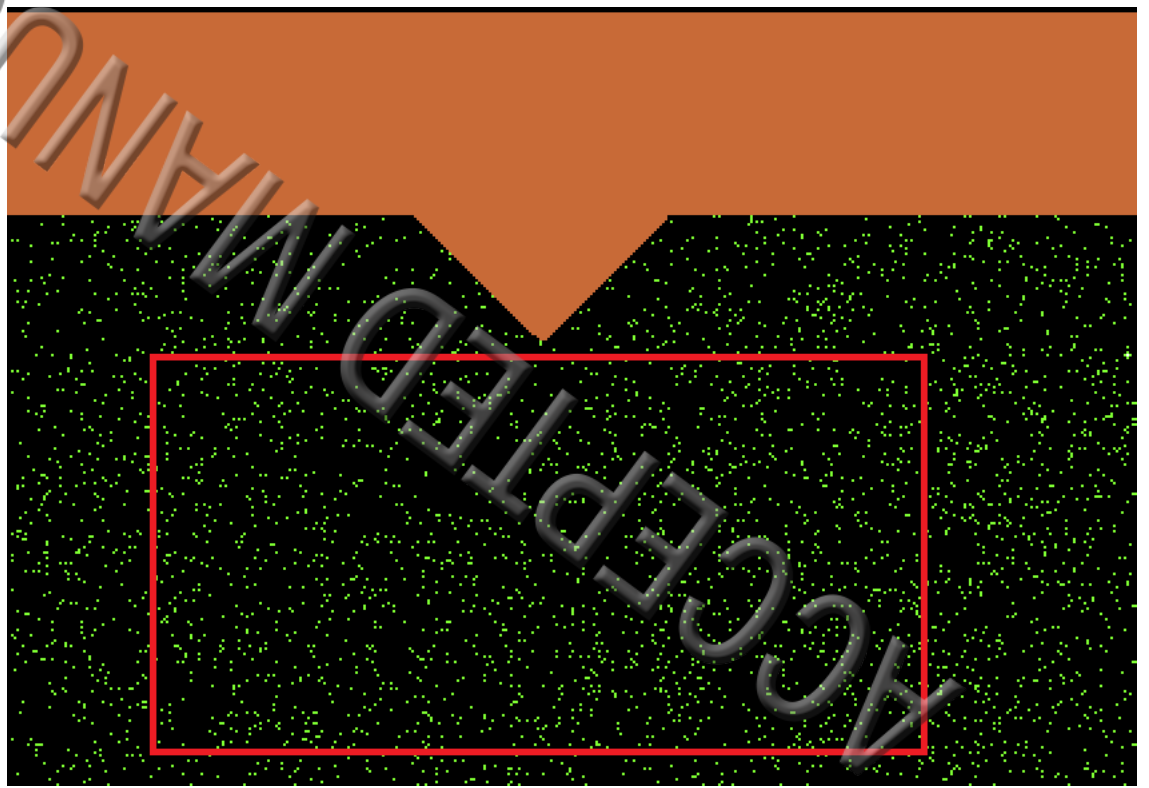
SCANNED MANUAL
ACCEPTED

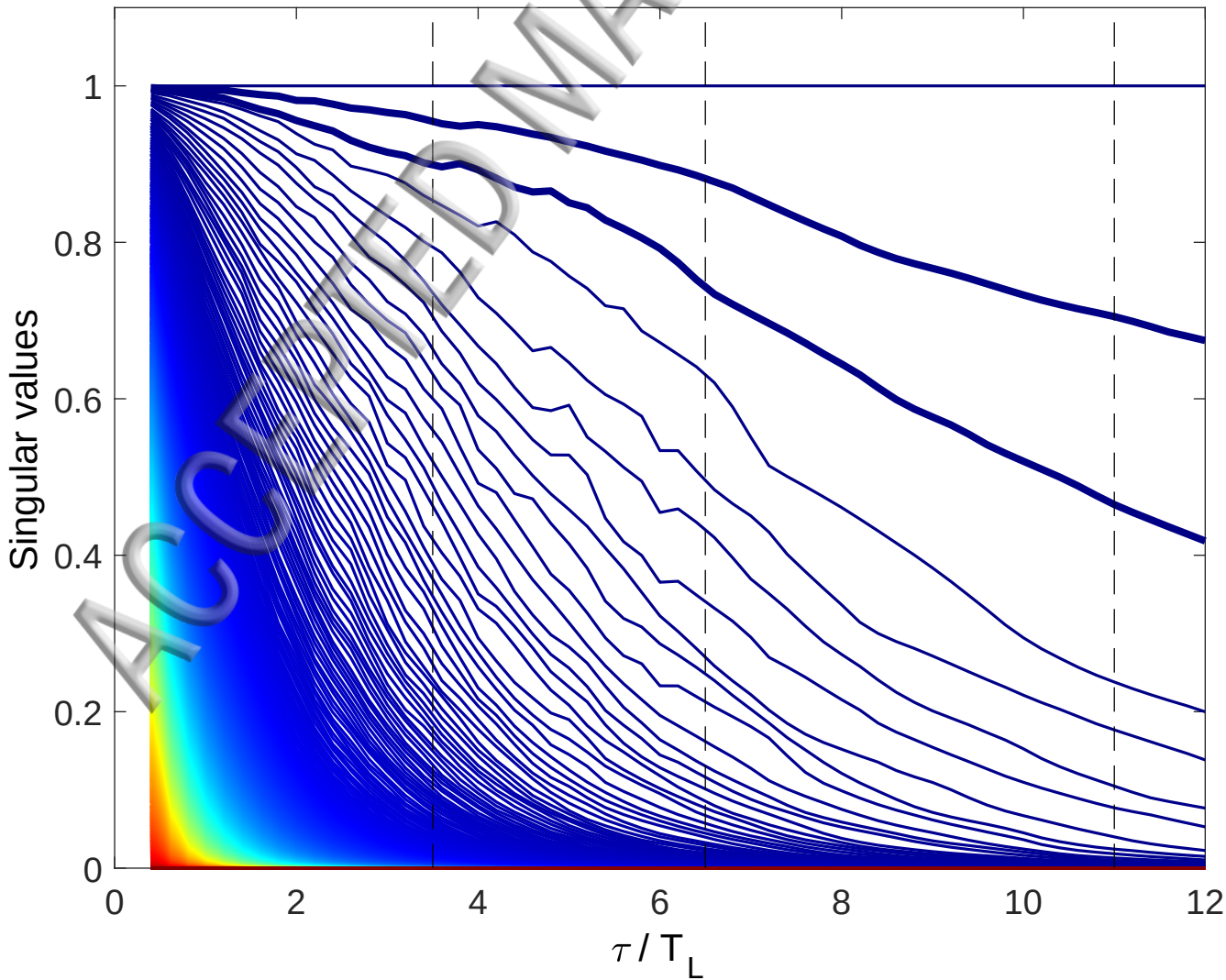

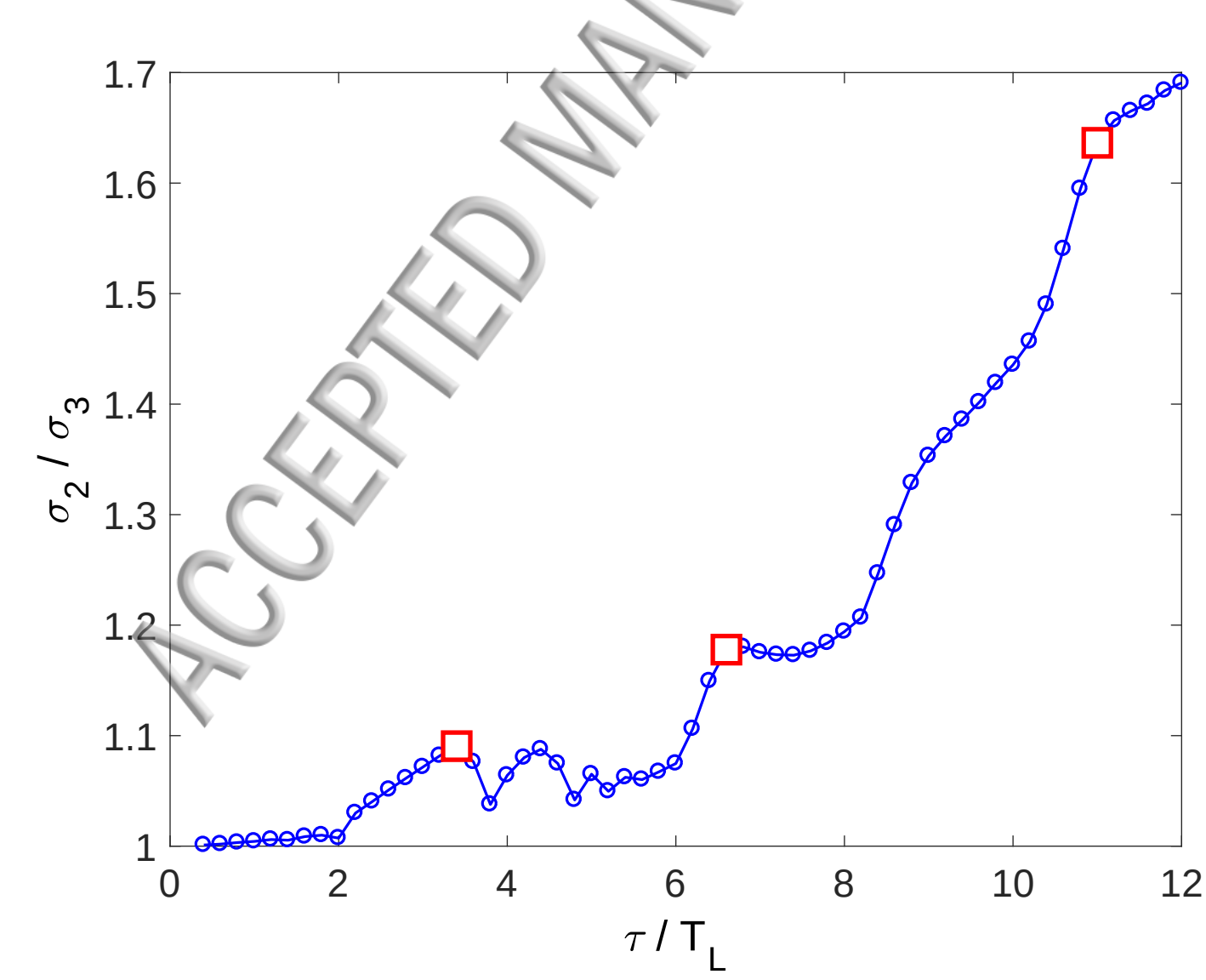

x

y

x

y

1

0.5

0

-0.5

-1

x

y

x

y

1

0.5

0

-0.5

-1

17 July 2024 23:31:57